Ordered oxygen-deficient superlattice from electron irradiation of biferroic $BiMnO_3$

H. Yang, Z. H. Chi, F. Y. Li, C. Q. Jin, and R. C. Yu*

Laboratory for Extreme Condition Physics, Beijing National Laboratory for Condensed Matter Physics, Institute of Physics, P.O. Box 603, Beijing 100080, People's Republic of China

(Received 21 October 2005; revised manuscript received 8 December 2005; published 26 January 2006)

The structural evolution of biferroic $BiMnO_3$ caused by electron-beam irradiation has been systemically studied by means of electron diffraction (ED), high-resolution transmission electron microscopy (HRTEM), electron energy-loss spectroscopy (EELS), and energy dispersive analysis of x-ray (EDX). The ED and HRTEM observations demonstrate clearly that the well-known $C2$ monoclinic form of $BiMnO_3$ is easily and irreversibly transformed to another modulated form by electron-beam irradiation. This irradiation-induced form shows an apparently higher symmetry and can be described by a body-centered pseudocubic superstructure with $a \approx b \approx c \approx 15.8$ Å and $\alpha \approx \beta \approx \gamma \approx 90°$. The EELS and EDX measurements reveal a small decrease of O/Mn ratio, but no change of Bi/Mn ratio in the irradiation-induced form as compared with the $C2$ monoclinic form. From the decrease of the O/Mn ratio, it can be concluded that the irradiation-induced form is produced from ordered oxygen deficiencies. A possible structure model is proposed.

DOI: 10.1103/PhysRevB.73.024114 PACS number(s): 72.10.Di, 68.37.Lp, 61.72.Ji, 77.80.Bh, 61.80.Lj

I. INTRODUCTION

Multiferroic materials, displaying simultaneously ferromagnetism and ferroelectricity, have recently attracted growing interest due to their intriguing physical properties and potential applications.[1,2] One of the extensively studied multiferroics is the perovskite-type $BiMnO_3$. The initial interest in the study of $BiMnO_3$ is mainly because it displays unexpected ferromagnetic behaviors with a Curie temperature (T_c) of ~105 K.[3] The ferromagnetism has been confirmed by many works.[4–7] Recently, theoretical calculations suggested that the perovskite-type $BiMnO_3$ is also expected to be ferroelectric.[8,9] Although ferroelectricity is difficult to observe due to the low resistance of films and the lack of large high-quality bulk samples, experimental evidence for the possible occurrence of magnetoferroelectricity in $BiMnO_3$ has been reported by Moreira dos Santos *et al.*[5] and Kimura *et al.*[10]

Multiferroic materials are rare in nature because the physical/structural/chemical conditions for a material to be simultaneously ferromagnetic and ferroelectric are generally difficult to be achieved.[9,11] Especially, ferroelectricity requires that the crystal structure be noncentrosymmetric and the ferroelectric transition is directly related to the structural phase transformation. Therefore, in such intriguing multiferroics, structural characterizations are extremely important. At room temperature, the noncentrosymmetric $BiMnO_3$ was primitively determined to be of a triclinically distorted lattice with $a=c \approx 3.935$ Å, $b \approx 3.989$ Å, $\alpha=\gamma \approx 91.47°$, and $\beta \approx 91.97°$.[12] Later, an accurate structural analysis based on powder neutron diffraction suggested that $BiMnO_3$ crystallizes in a monoclinic superstructure with a space group $C2$ and the lattice parameters $a=9.53$ Å, $b=5.61$ Å, $c=9.85$ Å, and $\beta=110.67°$.[13] This $C2$ monoclinic superstructure, which was confirmed by a later neutron-diffraction study,[14] is commonly accepted. Below room temperature, the monoclinic phase appears to be stable.[10,13,14] Successive structural changes have been reported to occur above room temperature.[7,10] With increasing temperature, the $C2$ monoclinic phase transforms reversibly to another $C2$ monoclinic phase at ~450 K, then irreversibly to a *Pbnm* orthorhombic phase at ~770 K, at which a ferroelectric phase transition likely occurs in terms of crystallography. However, the crystallographic data of the midtemperature monoclinic phase and the high-temperature orthorhombic phase are still absent yet.

Although it is well established that the perovskite-type $BiMnO_3$ forms a $C2$ monoclinic superstructure (hereinafter denoted as **I**) at room temperature, the existence of a room-temperature polymorphism of $BiMnO_3$ was also reported by some authors.[15,16] By means of ED and HRTEM, Chiba *et al.*[15] and Montanari *et al.*[16] observed in their high-pressure synthesized $BiMnO_3$ samples another modulated phase (hereinafter denoted as $\mathbf{I}^*$), which is different from the $C2$ monoclinic form. They suggested that the modulated phase $\mathbf{I}^*$ coexists with the $C2$ monoclinic form as another polymorph of $BiMnO_3$. However, the origin of this phase was not mentioned in their papers. In order to reveal the origin and further the characteristics of the form $\mathbf{I}^*$, recently we have undertaken a careful investigation, by means of ED, HRTEM, EELS, and EDX, on a highly pure $BiMnO_3$ sample obtained by the high-pressure synthesis method.[17] It is surprising and interesting that in our sample the form $\mathbf{I}^*$ was found to come just from the $C2$ monoclinic form **I** due to the electron-beam irradiation, and its formation is ascribed to the ordered oxygen deficiencies.

II. EXPERIMENTS

Using Bi_2O_3 (Alfa Aesar 99.99%) and Mn_2O_3 (Alfa Aesar 98%) as starting materials, polycrystalline $BiMnO_3$ specimen was synthesized at 1173 K and 5 GPa for 30 min. Details of the sample preparation have been described in Ref. 17. Thin foils for TEM studies were prepared by crushing the bulk specimen in an agate mortar filled with alcohol, and then dispersing the fine fragments suspended in alcohol on a mi-

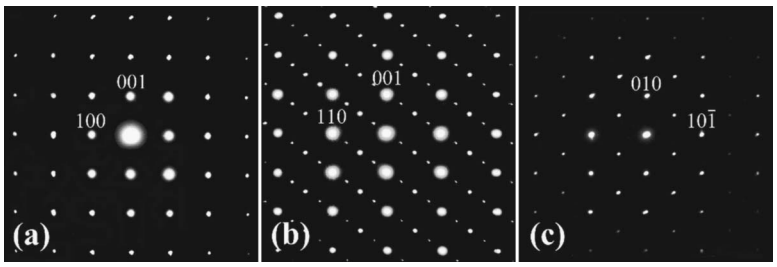

FIG. 1. Selected area ED patterns of the $C2$ monoclinic modulated form **I** along (a) $[010]_p$, (b) $[\bar{1}10]_p$, and (c) $[101]_p$ zone axes. The indices and zone axes are given in the fundamental perovskite subcell.

crogrid. A Tecnai F20 electron microscope with a field emission gun installed at Beijing Laboratory of Electron Microscopy, Beijing National Laboratory for Condensed Matter Physics, was used for ED, HRTEM, EELS, and EDX experiments. All the TEM studies were carried out at an acceleration voltage of 200 keV.

III. RESULTS AND DISCUSSION

The modulated phase $\mathbf{I}^*$ reported in Refs. 15 and 16 was said to show clear differences in structure from the $C2$ monoclinic modulated form **I** and could be easily distinguished by the ED technique. Unfortunately, we failed to find, in about the first two hours of TEM observations, a grain with the modulated structure $\mathbf{I}^*$, although a large number of grains had been examined. All the grains observed exhibit the $C2$ monoclinic structure **I**, as shown by some zone-axis ED patterns given in Fig. 1 (in this paper all the indices and zone axes are given with reference to the fundamental perovskite subcell). However, we continued to search for the grains of the phase $\mathbf{I}^*$ by ED. It was exciting that with the continuance of the TEM work we could occasionally observe certain grains exhibiting the modulated structure $\mathbf{I}^*$, but their superstructure spots were usually very weak. When our TEM work went on about five hours, the form $\mathbf{I}^*$ was visible very frequently. The experimental results showed clearly that in our sample the form $\mathbf{I}^*$ could appear and develop during our TEM observations due to the electron-beam irradiation, and was not an intrinsic polymorph of $BiMnO_3$ formed at high temperature and high pressure. The evolution of this modulated structure will be described in detail in the following. In addition, no TEM evidence shows the existence of a nonmodulated triclinic phase in our sample.

Here we first characterize the form $\mathbf{I}^*$. A series of ED patterns of this form were obtained, as shown in Fig. 2. All the patterns are indexed with reference to the fundamental perovskite subcell. It can be seen that the basic reflection spots, coupled with commensurate superstructure spots, display an apparently higher symmetry (pseudocubic), which is consistent with the observation by Montanari *et al.*[16] In fact, the three zone axes $[100]_p$, $[010]_p$, and $[001]_p$ of the fundamental perovskite substructure cannot be differentiated from one another by the ED patterns. Based on these ED patterns, the reciprocal lattice of this phase has been reconstructed and a part of it is schematically shown in Fig. 3. It can be seen that the commensurate superstructure spots manifest a face-centered pseudocubic lattice. In this paper, the unit cell of the form $\mathbf{I}^*$ is taken to be pseudocubic since the ED patterns cannot provide a more precise result. The three reciprocal vectors a^*, b^* and c^* of the modulated structure are shown in Fig. 3. According to its systematic extinction conditions observed to be $h+k+l=2n$ in general, $k+l=2n$ for $(0hk)$ and $l=2n$ for $(00k)$, the form $\mathbf{I}^*$ can be characterized as a body-centered pseudocubic superstructure. The lattice parameters derived from the ED patterns in Fig. 2 are $a \approx b \approx c \approx 15.8$ Å and $\alpha \approx \beta \approx \gamma \approx 90°$.

As mentioned above, the form $\mathbf{I}^*$ was considered to result from the monoclinic form **I** by the electron-beam irradiation. In order to further confirm this idea, we have focused on the *in situ* observation on a single grain of the form **I** continuously exposed to the electron beam. Figure 4 displays a series of the *in situ* ED patterns along $[010]_p$ zone axis direction, showing clearly the appearance and development of the

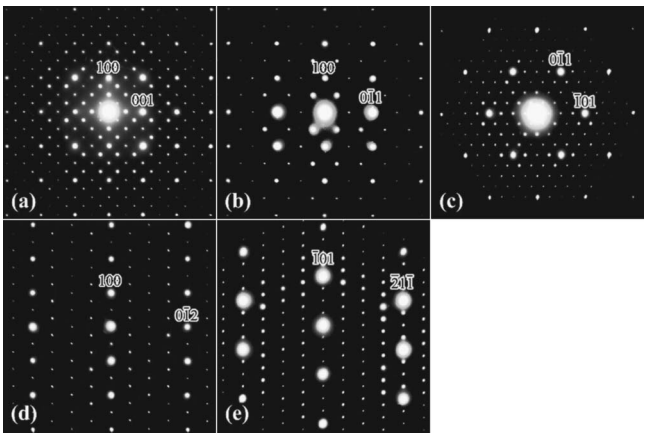

FIG. 2. Selected area ED patterns of the irradiation-induced modulated form $\mathbf{I}^*$ along (a) $[010]_p$, (b) $[011]_p$, (c) $[111]_p$, (d) $[021]_p$, and (d) $[131]_p$ zone axes. The indices and zone axes are given in the fundamental perovskite subcell.

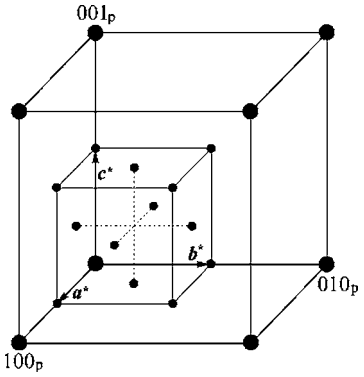

FIG. 3. A part of the reciprocal lattice of the form $\mathbf{I}^*$ reconstructed from the ED patterns in Fig. 2.

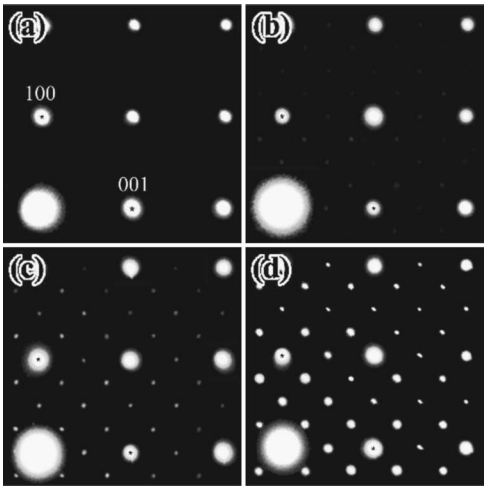

FIG. 4. *In situ* selected area ED patterns along the $[010]_p$ zone axis, showing clearly the appearance and development of the form $\mathbf{I}^*$: (a) the initial ED pattern; (b) recorded 20 min after (a); (c) recorded 5 min after (b); (d) recorded 5 min after (c).

modulated structure $\mathbf{I}^*$. It can be seen that in the initial ED pattern [Fig. 4(a)] only the fundamental Bragg reflections associated with the form **I** are present. After exposing the grain to the electron beam for about 20 min (in fact, the grain had been exposed to the electron beam for a few minutes before the first ED pattern was recorded), weak superstructure reflections related to the form $\mathbf{I}^*$ is visible in Fig. 4(b). With further increasing the irradiation time, the $\mathbf{I}^*$ superstructure reflections gradually become sharp and intense, as shown in Figs. 4(c) and 4(d). In addition, one can see from the ED patterns that the symmetry of the fundamental reflection spots gradually become higher (slightly from rhombic to tetragonal) with the appearance and development of the modulated structure $\mathbf{I}^*$. The picture showing that the form $\mathbf{I}^*$ is indeed developed from the form **I** by the electron-beam irradiation is supported by HRTEM studies. Figures 5(a)–5(c) illustrate the HRTEM images recorded from the same area irradiated for different duration of time, showing the detailed transition process from **I** to $\mathbf{I}^*$.

It should be noted that the transition to the modulated structure $\mathbf{I}^*$ is not simultaneous for all the grains, even in a single grain the transition occurs also not simultaneously in

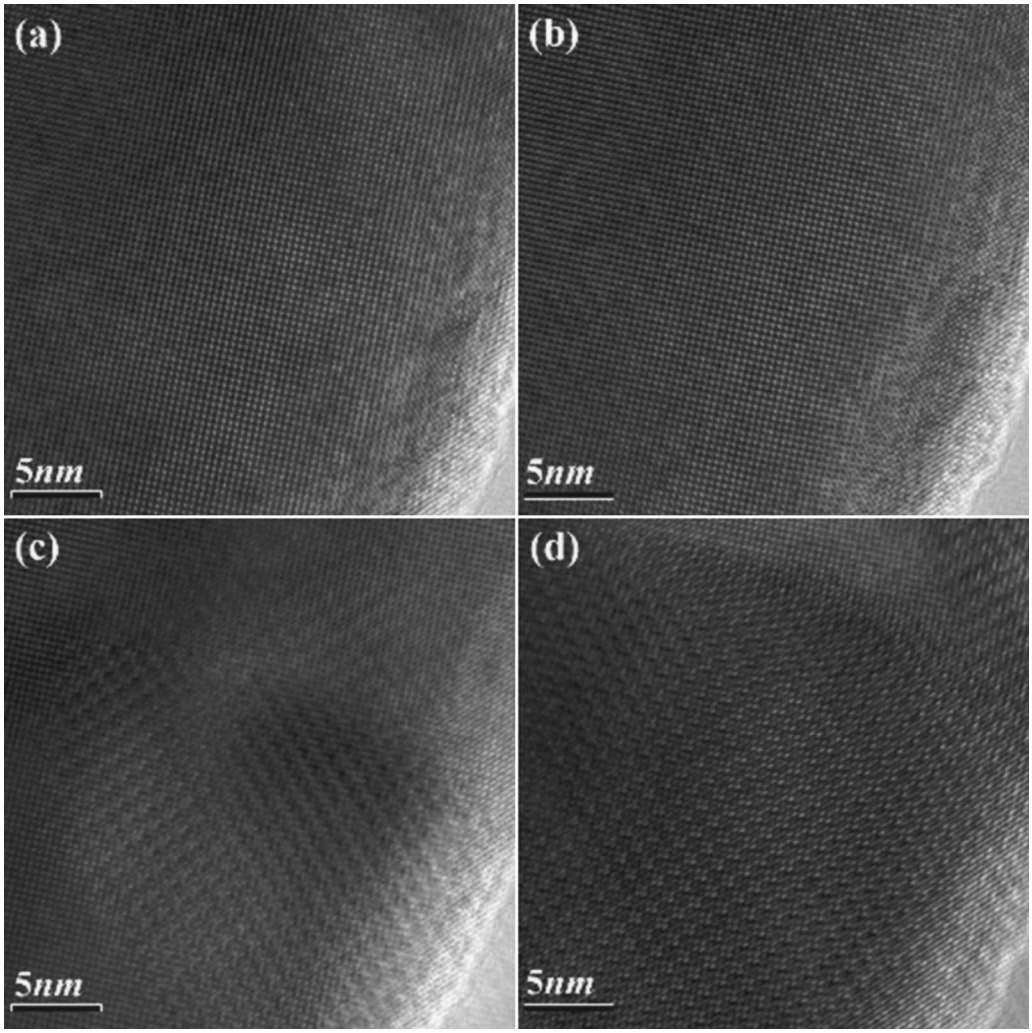

FIG. 5. HRTEM images recorded from the same area irradiated for different duration, showing the transition from **I** to $\mathbf{I}^*$: (a) the initial image; (b) recorded 12 min after (a); (c) recorded 5 min after (b); (d) recorded 3 min after (c).

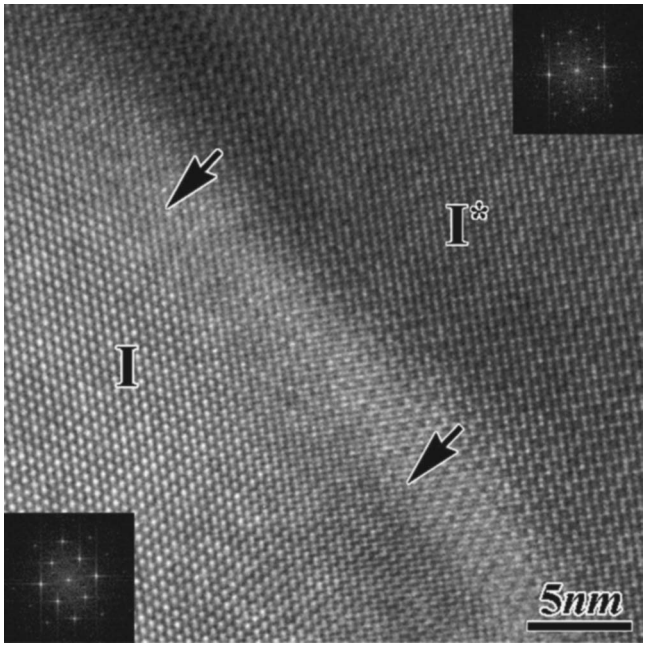

FIG. 6. HRTEM image taken along the $[011]_p$ zone axis, showing the coexistence of the forms **I** and **I***. As the coexisting region is continuously exposed to the electron beam, the form **I*** is clearly observed to extend gradually at the expense of the form **I** along the direction marked by arrows.

different regions. This is why we sometimes observe the form **I*** coexisting with the monoclinic form **I**. As an example, a HRTEM image showing the coexistence of the two forms is given in Fig. 6. When these coexisting regions are continuously exposed to the electron beam, the form **I*** is clearly observed to gradually extend at the expense of the form **I**. In Fig. 6, the black arrows show the advancing direction of the form **I***. In addition, we have found that the transition to the modulated structure **I*** is dependent on the electron-beam intensity. The transition in an intense electron beam is obviously faster than in the weak beam.

In order to see whether the irradiation-induced form **I*** is a stable phase, we have reexamined the sample after one month, and found that this form remains and no change is observed. With a long-time exposition to the electron beam, no matter whether intense or weak, the form **I*** is also found to be stable (at least no obvious change can be observed for 30 min irradiation).

In order to further reveal the origin of the form **I***, an attempt was made to compare its composition with that of the form **I** to see whether it is the chemical reaction that leads to its formation. It is well known that EELS is suitable for determining light element contents, while for heavy elements, EDX measurement can give precise results. In our experiments, combinative composition analyses by means of EELS and EDX have been used to determine the compositions of the forms **I** and **I***. The grains of **I*** used in measurement are those well developed, while the grains of **I** are those without long-time exposition to the electron beam. Of each form, ten different grains have been measured. The average O/Mn ratios for **I** and **I*** from EELS quantifications are, respectively, 3–0.002 and 3–0.036, showing a decrease

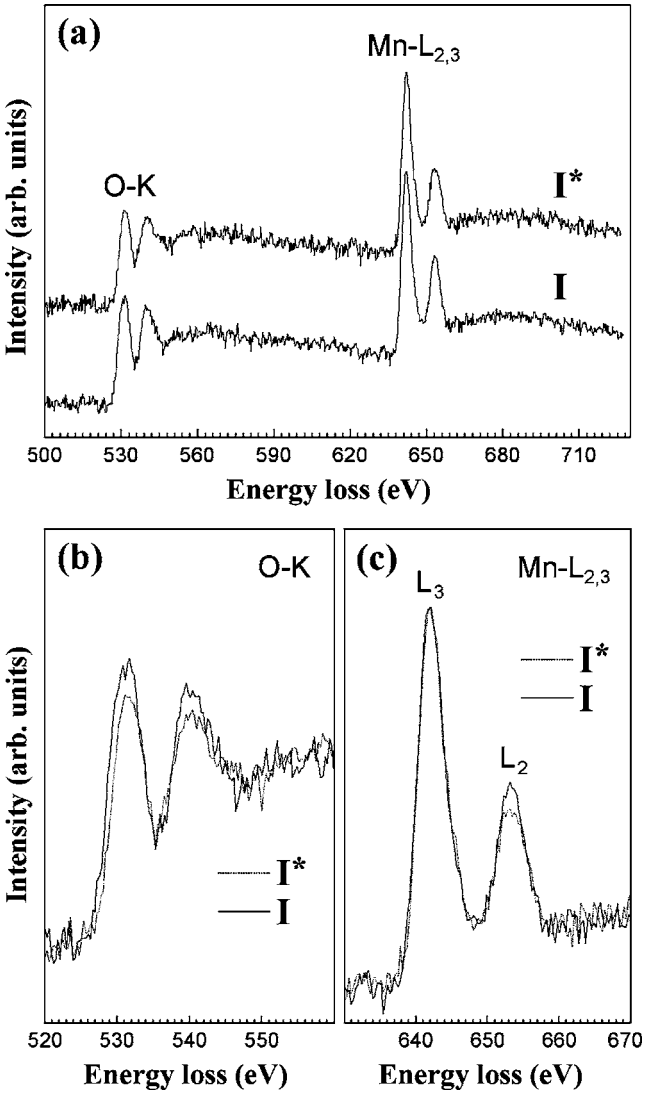

FIG. 7. (a) Typical EELS spectra obtained from the forms **I** and **I***. (b) Enlarged O-K edges. (c) Enlarged Mn-$L_{2,3}$ edges.

by 1.1% in the form **I*** as compared to the form **I**, while the Bi/Mn ratios of the two forms from TEM-EDX quantifications show no difference and their values are both equal to 1. Figure 7(a) shows the typical EELS spectra obtained from the two forms and each spectrum includes the O-K and Mn-$L_{2,3}$ absorption edges. The enlarged O-K and Mn-$L_{2,3}$ edges are shown in Figs. 7(b) and 7(c), respectively. To obtain the enlarged O-K edges, we normalize the two spectra from **I** and **I*** in Fig. 7(a) to have the same Mn-$L_{2,3}$-integrated counts. The enlarged O-K edges show clearly that the O-K edge obtained from the form **I*** is lower than that obtained from the form **I**, indicating that some oxygens are lost in the former. This result is reinforced by comparing the Mn-$L_{2,3}$ edges obtained from the two forms. From Fig. 7(c) one can see that the L_3/L_2 intensity ratio for the form **I*** is slightly higher than that for the form **I**, indicating that the manganese in the former shows up a lower valence state according to the known relationship between the L_3/L_2 ratio and the valence state for Mn ions.[18] The Mn-$L_{2,3}$ EELS results also suggest that the decrease of oxygen content in the irradiation-induced

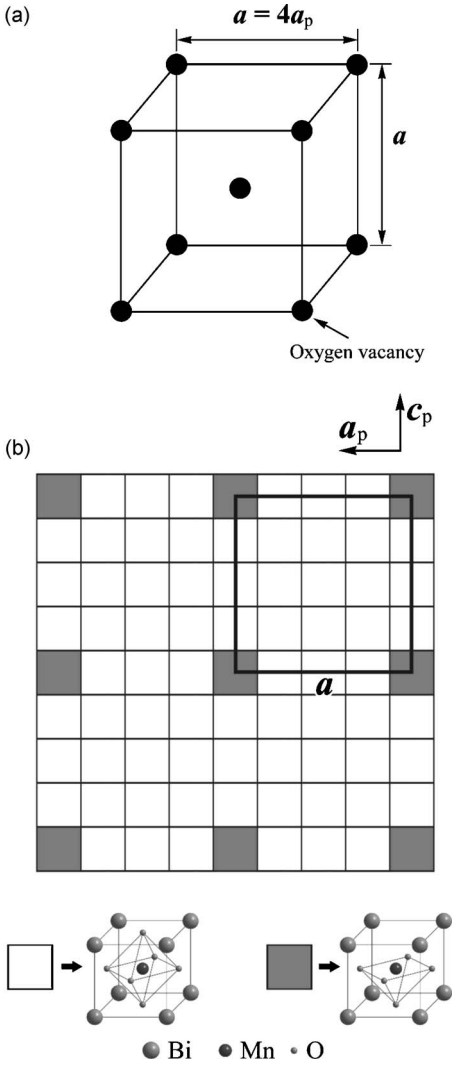

FIG. 8. An idealized structure model proposed for the form $\mathbf{I}^*$. (a) The space lattice constructed by only oxygen vacancies, showing a body-centered cubic lattice with a $4a_p$ supercell. (b) The distribution of the oxygen vacancies viewed along the $[010]_p$ direction. Here, the oxygen vacancies are assumed to be located in the a_pc_p plane of the fundamental perovskite structure.

form $\mathbf{I}^*$ as compared with the form $\mathbf{I}$. Therefore, the origin of the form $\mathbf{I}^*$ can be explained as follows. The electron-beam irradiation causes the perovskite-type $BiMnO_3$ to lose oxygen, resulting in the transition from the monoclinic form $\mathbf{I}$ to the body-centered pseudocubic form $\mathbf{I}^*$, and the formation of the latter is related to the ordered arrangement of oxygen deficiencies.

The EELS results suggest that there are about two oxygen vacancies in one supercell of the irradiation-induced form $\mathbf{I}^*$. Assuming that one supercell contains just two oxygen vacancies, an idealized structure model can be proposed as follows: the oxygen vacancies are distributed in a body-centered cubic framework in an ideal cubic perovskite structure of $BiMnO_3$. The space array constructed by only oxygen vacancies is schematically displayed in Fig. 8(a), showing the body-centered cubic lattice with a $4a_p$ supercell. A clearer picture about the distribution of the oxygen vacancies is depicted in Fig. 8(b). In this model, the oxygen vacancies are assumed to be located in the a_pc_p plane of the fundamental perovskite structure. From the proposed model, the HRTEM images are simulated using the simulation program *X-Win* 32. The simulated images along $[010]_p$ and $[111]_p$ zone axes are embedded on the bottom right-hand corner of the experimental ones and presented in Figs. 9(a) and 9(b), respectively. It is clear that the simulated images are in good agreement with the experimental ones, indicating that the proposed structural model is reasonable. It should be noted, however, that it is only an idealized structure model. In fact, the removal of oxygen will inevitably lead to a slight repulsion of the two positive Mn ions since two adjacent Mn atoms are always separated by an oxygen atom in a perfect structure. At the same time, the fundamental perovskite lattice is also slightly distorted, though the ED and the HRTEM images show clearly a pseudocubic lattice. More precise crystallographic data of the form $\mathbf{I}^*$ should be determined by x-ray powder diffraction or neutron diffraction experiments.

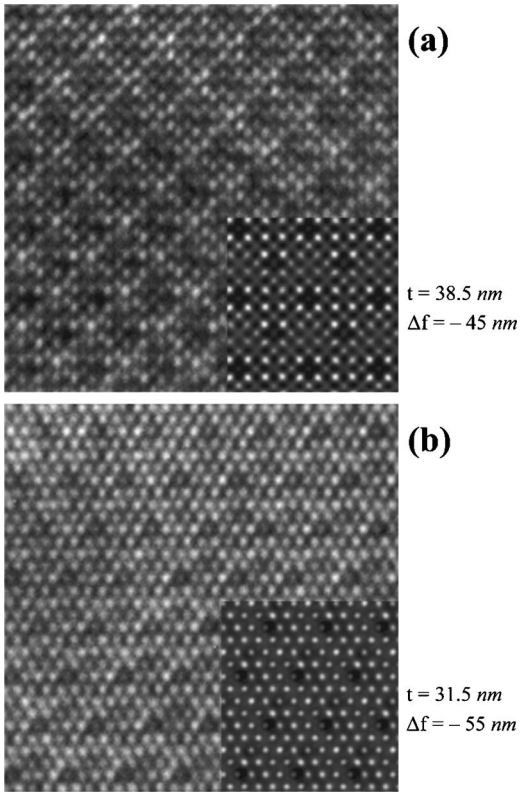

FIG. 9. Simulated HRTEM images. The simulated images along the (a) $[010]_p$ and (b) $[111]_p$ zone axes are embedded on the bottom right-hand corner of the experimental images.

Finally, we would point out that the magnetic measurements on our $BiMnO_3$ sample reveal, as expected, a typical ferromagnetic transition (Ref. 17) that agrees with most of the reported results.[4–7] No evidence from the magnetic investigations indicates that the sample is of a polyphasic nature, as reported in Ref. 16. The ferromagnetic results could exclude the possibility of the presence of the form $\mathbf{I}^*$ from the beginning in our high-pressure sample, which agrees with the TEM results, i.e., the form $\mathbf{I}^*$ is developed just from the form $\mathbf{I}$ under the electron-beam irradiation. Here we should

point out that the electron-beam irradiation is not necessarily the only way to produce the form $\mathbf{I}^*$ although in our sample the form $\mathbf{I}^*$ was revealed to be produced in this way. Since the form $\mathbf{I}^*$ is associated with the ordered oxygen deficiencies, any factor that induces oxygen deficiency, such as the inhomogeneity of chemical composition, could result in its formation. Since different experimental conditions (e.g., pressures, temperatures, sizes of the sample chamber, and the increase and decrease rates of temperature and pressure, etc.) might induce the deviation from the stoichiometric composition, the presence of the oxygen-deficient form $\mathbf{I}^*$ in some of the as-prepared samples, just like in the case reported by Montanari *et al.*,[16] is quite possible.

IV. CONCLUSIONS

We have carried out experiments to study the transition between the phases **I** and $\mathbf{I}^*$ of $BiMnO_3$. When exposed to the electron beam, the $C2$ monoclinic form **I** of $BiMnO_3$ is found to easily and irreversibly transform to a body-centered pseudocubic modulated form $\mathbf{I}^*$ with $a \approx b \approx c \approx 15.8$ Å and $\alpha \approx \beta \approx \gamma \approx 90°$. The EELS and EDX measurements reveal a small decrease of the O/Mn ratio, but no change of Bi/Mn ratio in the irradiation-induced form $\mathbf{I}^*$ as compared with the form **I**. From the decrease of the O/Mn ratio, the form $\mathbf{I}^*$ can be regarded to be a superstructure with ordered oxygen deficiencies. A possible structure model is also proposed.

ACKNOWLEDGMENTS

This work was supported by the National Natural Science Foundation of China (Grants No. 50471053, No. 50321101, No. 50332020, and No. 90401003) and the State Key Development Program for Basic Research of China (Grants No. 2005CB623602 and No. 2002CB613301).

*Corresponding author.

[1] A. J. Freedman and H. Schmid, *Magnetoelectric Interaction Phenomena in Crystals* (Gordon and Breach, London, 1975).
[2] G. Srinivasan, E. T. Rasmussen, B. J. Levin, and R. Hayes, Phys. Rev. B **65**, 134402 (2002).
[3] F. Sugawara, S. Iida, Y. Syono, and S. Akimoto, J. Phys. Soc. Jpn. **20**, 1529 (1965).
[4] A. F. Moreira dos Santos, A. K. Cheetham, W. Tian, X. Q. Pan, Y. F. Jia, N. J. Murphy, J. Lettieri, and D. G. Schlomb, Appl. Phys. Lett. **84**, 91 (2004).
[5] A. Moreira dos Santos, S. Parashar, A. R. Raju, Y. S. Zhao, A. K. Cheetham, and C. N. R. Rao, Solid State Commun. **122**, 49 (2002).
[6] E. Ohshima, Y. Saya, M. Nantoh, and M. Kawai, Solid State Commun. **116**, 73 (2000).
[7] H. Faqir, H. Chiba, M. Kikuchi, Y. Syono, M. Mansori, P. Satre, and A. Sebaoun, J. Solid State Chem. **142**, 113 (1999).
[8] R. Seshadri and N. A. Hill, Chem. Mater. **13**, 2892 (2001).
[9] N. A. Hill and K. M. Rabe, Phys. Rev. B **59**, 8759 (1999).
[10] T. Kimura, S. Kawamoto, I. Yamada, M. Azuma, M. Takano, and Y. Tokura, Phys. Rev. B **67**, 180401(R) (2003).
[11] A. N. Hill, J. Phys. Chem. B **104**, 6694 (2000).
[12] F. Sugawara, S. Iiida, Y. Syono, and S. Akimoto, J. Phys. Soc. Jpn. **25**, 1553 (1968).
[13] T. Atou, H. Chiba, K. Ohoyama, Y. Yamaguchi, and Y. Syono, J. Solid State Chem. **145**, 639 (1999).
[14] A. Moreira dos Santos, A. K. Cheetham, T. Atou, Y. Syono, Y. Yamaguchi, K. Ohoyama, H. Chiba, and C. N. R. Rao, Phys. Rev. B **66**, 064425 (2002).
[15] H. Chiba, T. Atou, H. Faqir, M. Kikuchi, Y. Syono, Y. Murakami, and D. Shindo, Solid State Ionics **108**, 193 (1998).
[16] E. Montanari, L. Righi, G. Calestani, A. Migliori, E. Gilioli, and F. Bolzoni, Chem. Mater. **17**, 1765 (2005).
[17] Z. H. Chi, C. J. Xiao, S. M. Feng, F. Y. Li, C. Q. Jin, X. H. Wang, R. Z. Chen, and L. T. Li, J. Appl. Phys. **98**, 103519 (2005).
[18] Z. L. Wang, J. S. Yin, and Y. D. Jiang, Micron **31**, 571 (2000).